GEOTHERMAL HEAT PIPES - JUST HOW LONG CAN THEY BE?

M.J. MCGUINNESS

Mathematics Department, Victoria University, Wellington

SUMMARY – Steady heat pipe solutions with capillarity and conduction effects included are considered. Phase plane trajectories of temperature vs. saturation typically approach zero capillarity solutions, one liquid-dominated and one vapor-dominated. Previous studies on the way in which choice of boundary conditions selects from these solutions are generalized, computer visualization techniques are used to cope with complexity, and accurate numerical solutions of the steady-state equations are presented. It has been speculated that the length of a gravity driven heat pipe may go to infinity. The maximum possible lengths of heat pipes are calculated here for a variety of values of the critical parameter, heat flow divided by permeability. It is found that liquid-dominated heat pipes can be more than 2 km long, and vapor-dominated heat pipes can be up to 100 km long in theory.

1 INTRODUCTION

In a heat pipe, it is possible to transfer heat with very little net mass flow, by having steam and liquid flowing in opposite directions, in contact with each other. In modeling a geothermal reservoir, the different densities of the liquid and vapor phases lead to a gravity-driven heat pipe, with liquid flowing down and vapor travelling up. Heat flow is vertically upwards, due to the specific enthalpy of steam being larger than that of liquid water. Although the system is open in general, it is typical that net mass flux is small. Such a model has been put forward by White *et al* [1] for a part of the Geysers steam field, and also applies to Larderello in Italy, Matsukawa in Japan, and Kawah Kamojang in Indonesia.

In a number of studies of the heat pipe mechanism, it has become clear that there are sometimes two solutions possible for a given steady gravity-driven heat flow, one vapor-dominated and one liquid-dominated ([14, 3, 4]). In a paper presented at the 1991 New Zealand Geothermal Workshop ([5]), it was stated that surface tension effects lead to narrow capillary boundary layers. Solutions typically track quickly from boundary values through a capillary-driven region onto the (outer) gravity-driven solutions. The directions taken by the boundary layer trajectories in the temperature-saturation plane were shown to determine which gravity-driven solution is tracked. A more detailed treatment may be found in [7].

These studies are extended here to more general relative permeability curves. Trajectories from accurate numerical integration of the steady-state equations are presented. The way that computer visualization graphics have helped the mathematical investigation is briefly indicated, and the results of integrating the pressure gradient along the outer solutions to obtain approximate estimates of the maximum possible heat pipe length are presented. Fuller mathematical details are in appendix A, and nomenclature is in appendix B.

2 STEADY-STATE EQUATIONS

The steady-state equations are presented here, under more general conditions than in previous studies. Relative permeability curves are not used except for illustration purposes, in an attempt to reach conclusions that clearly do not depend on the particular empirical choice of form for relative permeabilities.

A single-layer model of two-phase fluid flowing vertically, with zero net mass flow and a fixed net heat flow is used. Sign conventions are indicated in Fig. 1. This model allows in principle an infinite range of heat flow values, in contrast with two and three-layer models (e.g. [3, 6]), which limit heat flows to values that may be conducted across a quiescent single-phase layer. This limitation is significant. Allowing two-dimensional convection in an adjacent single-phase layer would be one justification for considering the more generous single-layer model.

Another limitation of previous studies has been an insistence on a smooth transition of saturation from steam to liquid single-phase values. Only trajectories that cross all the way from one side of the temperature-saturation plane to the other were allowed. This is an unnecessary restriction. Step changes in saturation between a two-phase region and a single-phase region satisfy thermodynamic equilibrium conditions, as saturation jumps on the pore scale are already present within the two-phase region. Provided mass and energy are conserved across any saturation jump, there is also no problem with for example steam phase velocity suddenly being zero, as the steam itself ceases to exist at the same place.

Darcy's law gives the momentum balance for the two phases,

$$u_l = -\frac{kk_{rl}}{\nu_l}\left(\frac{\partial P_l}{\partial z} + \rho_l g \sin\theta\right)$$
$$u_v = -\frac{kk_{rv}}{\nu_v}\left(\frac{\partial P_v}{\partial z} + \rho_v g \sin\theta\right).$$

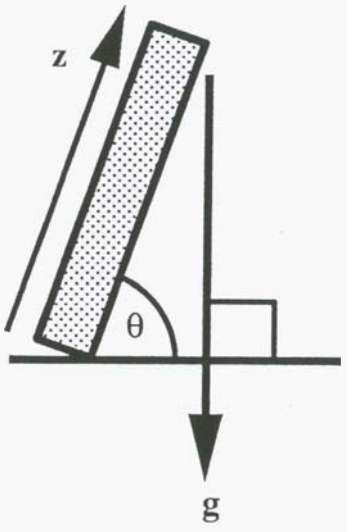

Figure 1. Sign conventions used in 1D heat pipe model

Capillary pressure is taken to be

$$P_c(S,T) = P_v - P_l,$$

and the particular form for P_c is kept general at this point. Vapor-pressure lowering (the Kelvin effect) is represented as (after [9])

$$P_v = f_{\rm vpl}(T,S)\, P_{\rm sat}(T) \qquad (1)$$

where the vapor-pressure lowering factor is approximated by

$$f_{\rm vpl} = \exp\left\{\frac{m_l P_c(S,T)}{\rho_l \mathrm{R}(T+273.15)}\right\},$$

and where $P_{\rm sat}$ is the saturated vapor pressure of bulk liquid, obeying the Clausius-Clapeyron relation

$$\frac{dP_{\rm sat}}{dT} = \frac{\rho_l \rho_v h_{vl}}{(T+273.15)(\rho_l - \rho_v)}.$$

Mass and energy conservation yield

$$u_l + u_v = 0,$$
$$u_v h_v + u_l h_l = Q + \lambda\frac{\partial T}{\partial z}.$$

See also [3, 4, 11] for these. Noting that Eqn. 1 implicitly relates T to P_v and S, and that P_c usually depends on P_v via T and on S, these conservation equations may be rearranged to obtain

$$\frac{\partial P_v}{\partial z} = -\frac{\mathcal{H}(P_v,S)}{\mathcal{F}(P_v,S)}, \qquad (2)$$
$$\frac{\partial S}{\partial z} = \frac{\mathcal{G}(P_v,S)}{\mathcal{F}(P_v,S)} \qquad (3)$$

where the right-hand sides are complicated functions of P_v and S, and are given in appendix **A.**

Hence steady-state solutions may usefully be plotted in the P_v, S (or T, S) phase plane, as the above are two coupled autonomous nonlinear first-order differential equations. Satik *et al* [6] study these equations with particular forms for capillary pressure (Leverett J-function), relative permeability (percolation) and the Clausius-Clapeyron equation (vapor phase as ideal gas).

3 BOUNDARY LAYERS

In [5] it was noted that $\mathcal{H}$ is typically much smaller than $\mathcal{G}$ in a geothermal reservoir. This may be formalized by factoring out a small parameter $\epsilon = \frac{1}{P_0}\frac{\partial P_c}{\partial S}$ in Eqns. 2 and 3, and rescaling z and P_v. The resulting equations are (details in appendix **A)**

$$\frac{\partial P_v}{\partial z} = -\frac{\mathcal{H}(P_v,S)}{\mathcal{F}(P_v,S)}, \qquad (4)$$
$$\epsilon\frac{\partial S}{\partial z} = \frac{\mathcal{G}(P_v,S)}{\mathcal{F}(P_v,S)}, \qquad (5)$$

and terms on the right-hand sides are now of the same sizes in both equations, provided thermal conduction is negligible compared to counterflow.

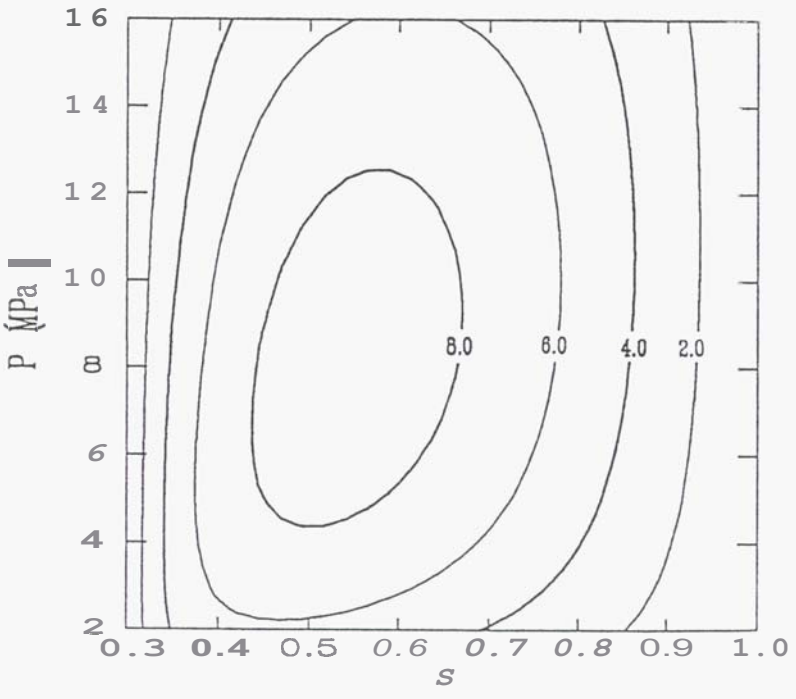

Figure 2. Level contours of $\mathcal{G} = 0$, k=1d, representing gravity-driven solutions. The contoured value is Q/k kW/d m^2.

Outer solutions are obtained by setting $\epsilon = 0$, and are the zero capillarity gravity-driven solutions given by the

level contours of the $\mathcal{G} = 0$ isosurface in the pressure-saturation plane. These have previously been referred to as the steady-state solvability conditions for gravity-driven heat pipes ([14]) in the absence of capillarity. They are plotted in Fig. 2 as contours of constant Q/k in the pressure-saturation plane, using linear relative permeability curves for illustration purposes, and $k = 1\mathrm{d}$. Similar contours are obtained when other choices of relative permeability curves are made, and for k values down to 1md. Below this permeability, heat flow due to conduction effects begins to be important, and the nature of these contours changes dramatically ([7], and see section 5).

Inner solutions are obtained by rescaling to $Z = z/\epsilon$, and again solving with $\epsilon = 0$, giving (to leading order) capillary-driven boundary layers of thickness ϵ with constant pressure and varying saturation, that approach the $\mathcal{G} = 0$ contours.

The size of ϵ may be estimated using the Leverett J-function approximation for capillary pressure ([10, 13]),

$$P_c = \frac{\sigma \cos\theta}{\sqrt{k}} J(S)$$

to be

$$\epsilon \sim 10^{-9}/\sqrt{k}.$$

This may be considered small when $k \gg 10^{-18}\mathrm{m}^2$. Since

$$\frac{\partial P_v}{\partial S} = -\epsilon \frac{\mathcal{H}}{\mathcal{G}},$$

ϵ is a measure of inner solution slopes in the pressure-saturation phase plane. Solution slopes are less than 10 when $k > 10^{-16}\mathrm{m}^2$.

4 NUMERICAL INTEGRATION & LENGTHS

The full steady-state equations 2 and 3 have been integrated numerically, using the package called STRIDE ([15]), an implementation of singly-implicit Runge-Kutta methods designed for both stiff and non-stiff systems of ordinary differential equations. Thermodynamic quantities have been accurately calculated using routines culled from TOUGH2 ([16]), which conform to the standards laid out in [17]. These numerical solutions confirm the above perturbation analysis of solution behaviour. They are plotted in Figs. 3 and 4 . Note how narrow the capillary boundary-layer regions are (typically a meter or two) compared with the gravity-driven regions (kilometers). The gravity-driven regions track closely the $\mathcal{G} = 0$ contours, the differences being indistinguishable when trajectories are plotted together with the zero capillarity contours in a pressure-saturation phase plane.

The plot for $k = 0.01\mathrm{md}$ is included to indicate the significantly different behaviour seen when conduction is important. As expected from the analysis, capillary boundary layers are no longer evident. The hotter end switches from being the vapor-dominated end to being the liquid-dominated end.

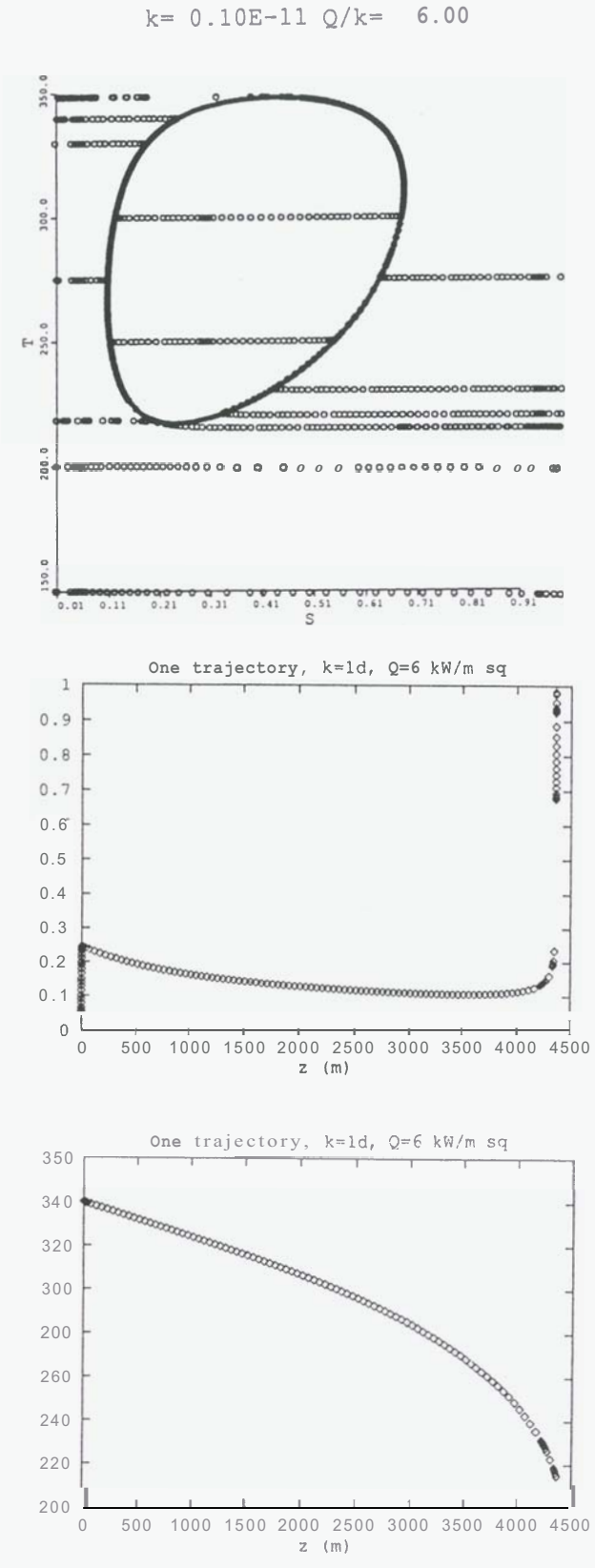

Figure 3. Steady solutions to the full heat pipe equations, calculated using STRIDE. Phase plane plots for $Q/k = 6\mathrm{kW/dm}^2$ and $k = 1d$ are shown, together with saturation vs. z and T vs. z for one of the trajectories.

These integrations give accurate values of heat pipe lengths also, for each particular trajectory. Previous studies(eg [8, 12]) have suggested infinite maximum possible lengths. These calculations were based on integrating the saturation equation 3 and ignoring pressure or temperature changes. This is ok in the boundary layers, but ignores the variation of the outer gravity-driven solutions $\mathcal{G} = 0$ with pressure or temperature.

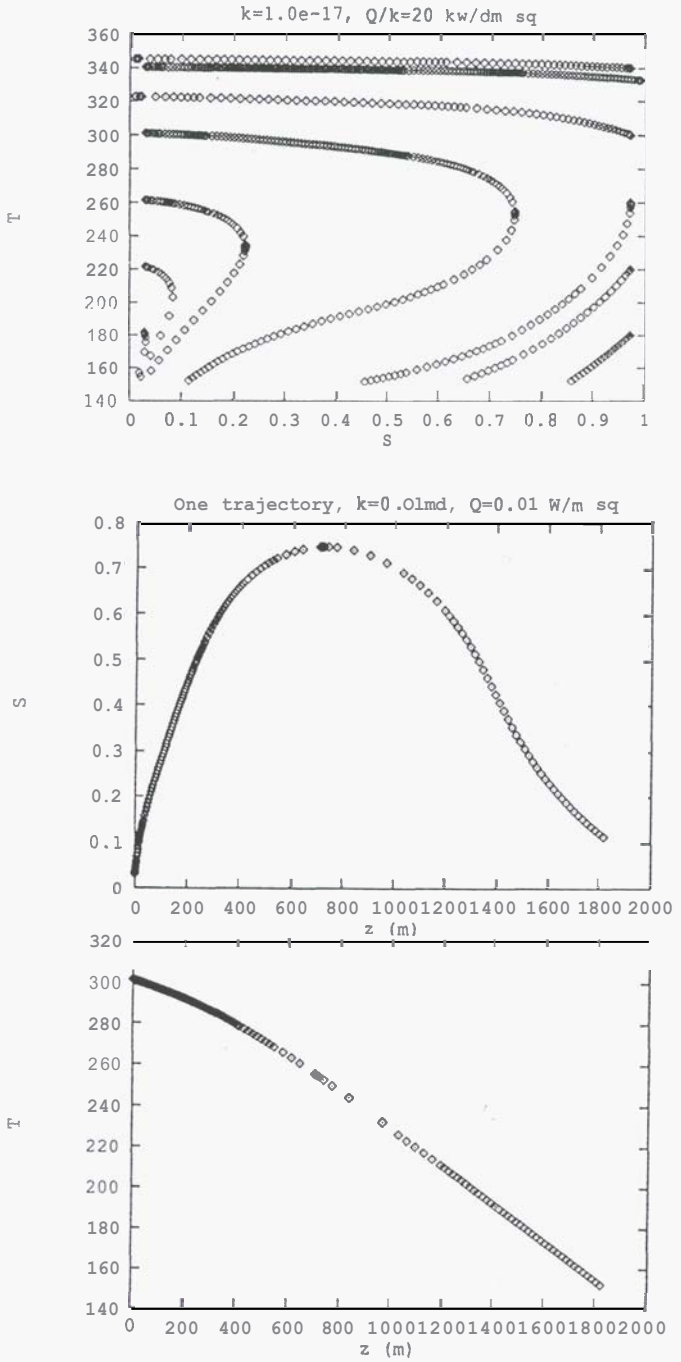

Figure 4. Steady solutions to the full heat pipe equations, calculated using STRIDE. Phase plane plots for $Q/k = 20\mathrm{kW/dm^2}$ and k = 0.01md are shown, together with saturation vs. z and T vs. z for one of the trajectories.

A alternative way to estimate maximum heat pipe length is to use only the outer gravity-driven solution, as this extends over much larger distances than the boundary layer, and to use quadrature to integrate the pressure derivative along the $\mathcal{G} = 0$ contour. In order to obtain the maximum possible length, integration proceeds from one end of a contour (low temperature) to the other end (high temperature). If a contour extends below 100°C, integration starts there, corresponding to a choice not to consider pressures below atmospheric. All contours can be shown to close up as the critical temperature is approached. In fact, the numerical routines used in this study do not apply to temperatures above 350°C, so this value has been used as a somewhat arbitrary cutoff point when necessary.

Outer solutions satisfy ([7])

$$\frac{\partial p}{\partial z} = -\frac{g(\lambda_l \rho_l + \lambda_v \rho_v)}{\lambda_l + \lambda_v},$$

$$Q = \frac{g \sin\theta [h_{vl}(\rho_l - \rho_v)\lambda_l \lambda_v + (\lambda_l \rho_l + \lambda_v \rho_v)\lambda \frac{dT}{dp}]}{\lambda_l + \lambda_v}$$

where z has been returned to its original dimension (m), and since there is negligible capillary pressure effect on the outer solution, there is only one pressure variable, p. The second equation follows directly from setting $\mathcal{G} = 0$. It can be used to relate pressure and saturation, allowing the solution of the first equation.

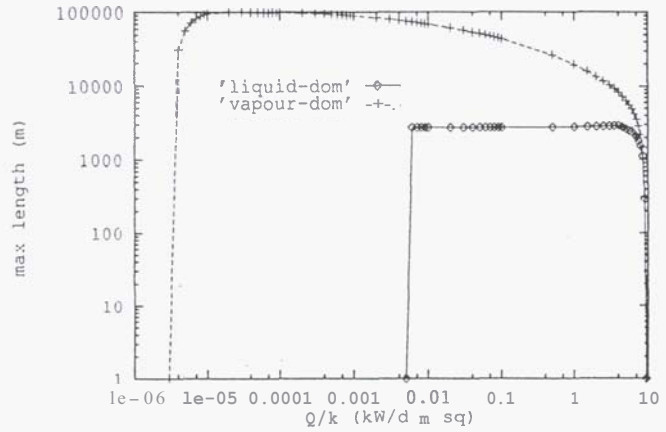

Figure 5. Maximum possible heat pipe lengths, calculated using the outer gravity-driven solutions.

Then heat pipe length may be calculated by integrating (noting that partial derivatives are ordinary derivatives given that solutions are steady):

$$L = \int_C dz = -\int_C \frac{\lambda_l + \lambda_v}{g(\lambda_l \rho_l + \lambda_v \rho_v)} dp,$$

where C corresponds to a choice of either the vapor-dominated branch or the liquid-dominated branch of the $\mathcal{G} = 0$ contour.

This has been accomplished using the adaptive mesh NAG routine D01AHF, with the results plotted in Fig. 5. Note that the vapor-dominated branches lead to potentially longer heat pipes, due to the smaller density of vapor giving slower pressure change along the heat pipe. Note also the different cutoff values of Q/k, higher for the liquid-dominated branches. These correspond to heat

flow dropping to conductive values, with the higher pressure gradient for a liquid-dominated heat pipe leading to a higher temperature gradient, and hence a larger conductive heat flow. Once heat flow drops to conductive values, convection or counterflow is not supported.

5 SCIENTIFIC VISUALIZATION

The right-hand sides of Eqns. **2** and **3** are complicated functions of the thermodynamic variables P_v and S, and also depend on values chosen for the parameters Q and k. The ability to visualize trajectory slopes in full colour three-dimensional views, (Q, P_v, S) with k as a possible fourth dimension, has been useful both in exploring possible relationships and in verifying the validity of the mathematics, for entire regions of the space rather than for particular numerical solutions. Black and white versions are reproduced here in Fig. 6 to give some indication of the information available. In this figure, linear relative permeabilities are used.

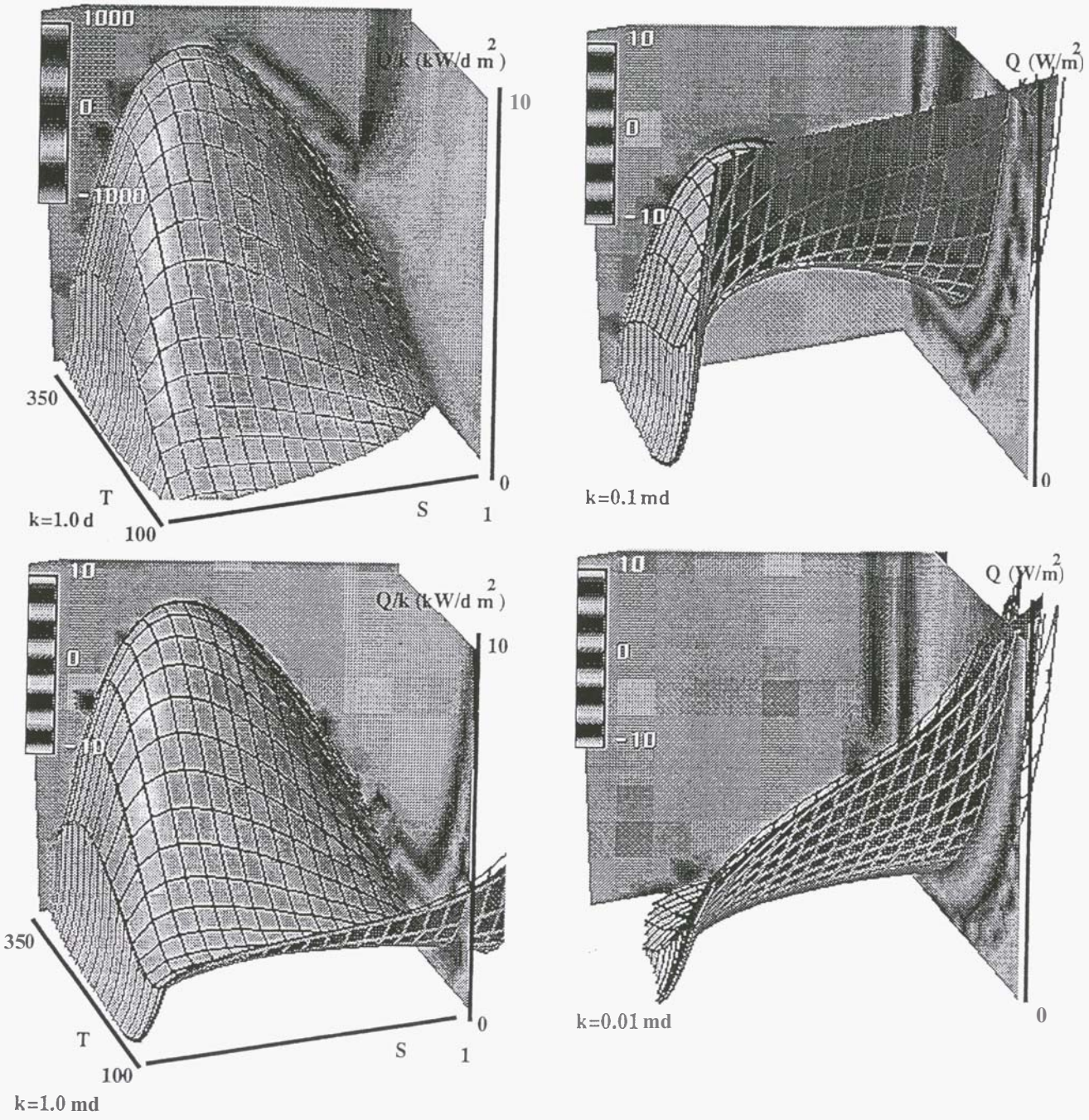

Figure 6. Computer visualizations of slopes for steady heat pipes. Axes have the same orientation for all plots, and the vertical axis has varying ranges.

In particular, isosurfaces through zero slope values are shown, where ***slope*** here means $\partial S/\partial T$. Zero values correspond to trajectories going vertical in figs. 5, and to the $\mathcal{G} = 0$ gravity-driven contours. The contours drawn near the isosurfaces are for slopes ± 0.5, to give some indication of the extent or thickness of nearly zero slopes. Another indication of the extent and range of slope values comes from the colour (!) coded slices shown. The legends apply to these slices. Note the movement from slopes of the order of 1000 for k near one darcy, to slopes of the order of 10 for k near 0.1 md.

When conduction effects are negligible, Q/k is a good vertical parameter to plot, reflecting the fact that the maximum amount of heat that a gravity-driven heat pipe will carry is proportional to permeability. As permeability drops in Fig. 6, the effect of conduction on the $\mathcal{G} = 0$ surface can be seen to be to curl it up from the cooler temperature end, and from the liquid-dominated corner. Heat flows reduce to conductive values, independent of k.

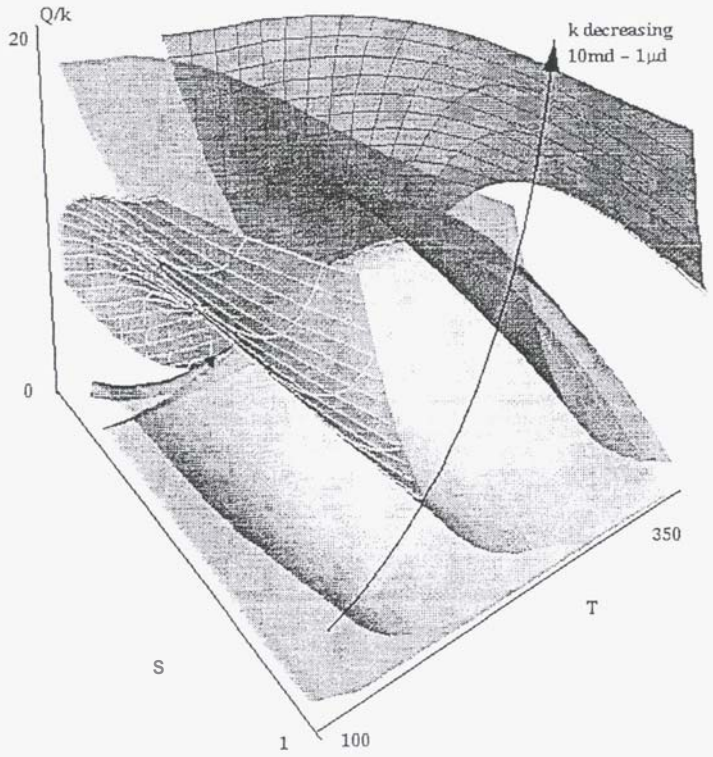

Figure 7. Another view of the visualization in Fig. 6, with a common Q/k axis and scale.

6 ACKNOWLEDGEMENTS

I am grateful to the Internal Grants Committee of Victoria University of Wellington, and to the New Zealand Lottery Grants Board, for their financial assistance enabling the use of a Silicon Graphics Iris Indigo workstation with the Iris Explorer visualization package, to explore and verify the mathematical insights in this paper.

I am also grateful to Professor J. Harper and I. Pestov of Victoria University, and to my former DSIR colleagues now in the Applied Maths Group at IRL, for many helpful discussions.

References

[1] D.E. White, J.P. Muffler, and A.H. Truesdell, Vapor-dominated hydrothermal systems compared with hot-water systems, *Economic Geology,* **66** 75–97 (1971).

[2] M.J. McGuinness, M. Blakeley, K. Pruess, and M.J. O'Sullivan, Geothermal Heat Pipe Stability: Solution Selection by Upstreaming and Boundary Conditions, *Transport in Porous Media* **11**,71–100 (1993).

[3] G. Schubert and J.M. Strauss, Steam-water Counterflow in Porous Media, *J. Geophys. Res.* **84** 1621–1628 (1979).

[4] R. McKibbin, and K. Pruess, Some effects of non-condensible gas in geothermal reservoirs with steam-water counterflow, *Geothermics,* **18** No.3, 367–375 (1989).

[5] M.J. McGuinness, Solution selection in geothermal heat pipes, presented at the 13th New Zealand Geothermal Workshop (1991), and published in *the proceedings of the 14th New Zealand Geothermal Workshop,* Auckland University, November 1992, pp.321–326.

[6] C. Satik, M. Parlar, and Y.C. Yortsos, A Study of Steady-state Steam-water Counterflow in Porous Media, *Int. J. Heat and Mass Transfer,* **34** No.7, 1755–1772 (1991).

[7] M.J. McGuinness, Steady Solution Selection and Existence in Geothermal Heat Pipes, in preparation for submission to *Int. J. Heat and Mass Transfer,* Nov 1993.

[8] C.H. Sondergeld and D.L. Turcotte, An experimental study of two-phase convection in a porous medium with applications to geological problems, *J. Geophys. Res.,* **82,** No.14, 2045–2053 (1977).

[9] N.E. Edlefsen, and A. B. C. Anderson, Thermodynamics of Soil Moisture, *Hilgardia,* **15** No.2, 231-298 (1948).

[10] M.C. Leverett, Capillary behaviour in porous solids, *AIME Transactions,* **142** p.52 (1941).

[11] J.C. Martin, R.E. Wegner and F.J. Kelsey, One-dimensional convective and conductive geothermal heat flow, *Proc. 2nd Workshop on Geothermal*

Reservoir Engineering, Stanford University, pp.251–262 (1976).

[12] K.S. Udell, Heat Transfer in Porous Media Considering Phase Change and Capillarity — the Heat Pipe Effect,

[13] **K.S.** Udell, Heat Transfer in Porous Media heated from above with evaporation, condensation, and capillary effects, *J. Heat Transfer,* 105 485–492 (1983).

[14] M.J. McGuinness, M. Blakeley, K. Pruess, and M.J. O'Sullivan, Geothermal Heat Pipe Stability: Solution Selection by Upstreaming and Boundary Conditions, *Transport in* **Porous** *Media* **11**, 71–100 (1993).

[15] J.C. Butcher, K. Burrage, F.H. Chipman, STRIDE Package for Differential Equations, Mathematics Department, University of Auckland, New Zealand, email **chipman@mat.aukuni.ac.nz**, 1991.

[16] K. Pruess, SHAFT, MULKOM, TOUGH: a set of numerical simulators for multiphase fluid and heat flow, *Geotermia, Rev. Mex. Geoenergia* **4** (1), 185–202 (1988).

[17] T. Sato, T. Minamiyamaand J. Yata, A formulation of the thermodynamic properties of ordinary water substance, *Kyoto University Faculty of Engineering Memoirs,* **29** Part 1, 16–27 (Jan 1967).

A SOME MATHEMATICS

Mass and energy conservation yield

$$\begin{aligned} u_l + u_v &= 0, \\ u_v h_v + u_l h_l &= Q + \lambda \frac{\partial T}{\partial z}. \end{aligned}$$

Rearrangement gives

$$\begin{aligned} \frac{\partial P_v}{\partial z} &= -\frac{\mathcal{H}(P_v, S)}{\mathcal{F}(P_v, S)}, \\ \frac{\partial S}{\partial z} &= \frac{\mathcal{G}(P_v, S)}{\mathcal{F}(P_v, S)} \end{aligned}$$

where

$$\begin{aligned} \mathcal{F} &= F_1 F_4 - F_3 F_2, \\ \mathcal{G} &= G_1 G_4 - G_3 G_2, \\ \mathcal{H} &= H_1 H_4 - H_3 H_2, \end{aligned}$$

and

$$\begin{aligned} F_1 &= \lambda_l + \lambda_v - \lambda_l \frac{\partial P_c}{\partial P_v}, \\ F_2 &= \mathrm{Ai} \frac{\partial P_c}{\partial S}, \\ F_3 &= \lambda_l h_l + \lambda_v h_v - \lambda_l h_l \frac{\partial P_c}{\partial P_v} + \mathrm{A} \frac{\partial T}{\partial P_v}, \\ F_4 &= \lambda_l h_l \frac{\partial P_c}{d\,\widehat{s}} - \mathrm{A} \frac{\partial T}{d\,s}, \end{aligned}$$

$$\begin{aligned} G_1 &= F_1 \\ G_2 &= g \sin\theta (\lambda_l \rho_l + \lambda_v \rho_v), \\ G_3 &= F_3, \\ G_4 &= Q + g \sin\theta (\lambda_l \rho_l h_l + \lambda_v \rho_v h_v), \\ H_1 &= G_2, \\ H_2 &= F_2, \\ H_3 &= G_4, \\ H_4 &= F_4. \end{aligned}$$

The structure of these equations is simplified a little if the factor $\frac{\partial P_c}{\partial S}$ is extracted from the right-hand sides, and z is rescaled by a maximum pressure P_0 so that pressure is of order one:

$$\begin{aligned} \frac{\partial P_v^*}{\partial z^*} &= -\frac{\mathcal{H}^*(P_v^*, S)}{\mathcal{F}^*(P_v^*, S)}, \\ E\frac{\partial S}{dz^*} &= \frac{\mathcal{G}^*(P_v^*, S)}{\mathcal{F}^*(P_v^*, S)} \end{aligned}$$

where (in the development in the main body of the paper. the asterisks are dropped):

$$\begin{aligned} \mathcal{F}^* &= \left[\lambda_l \left(1 - \frac{\partial P_c}{\partial P_v}\right) + \lambda_v\right] \left(\lambda_l h_l - \frac{\lambda}{\frac{\partial P_c}{\partial S}} \frac{\partial T}{\partial S}\right) \\ &\quad -\lambda_l \left(\lambda_l h_l + \lambda_v h_v - \lambda_l h_l \frac{\partial P_c}{\partial P_v} + \lambda \frac{\partial T}{\partial P_v}\right), \\ \mathcal{G}^* &= g \sin\theta \left[\lambda_l \lambda_v \left(-(\rho_l - \rho_v) h_{vl} - \rho_v h_{vl} \frac{\partial P_c}{\partial P_v}\right)\right. \\ &\quad +\lambda_l \left(1 - \frac{\partial P_c}{\partial P_v}\right) \left(\frac{Q}{g \sin\theta} - \lambda \rho_l \frac{\partial T}{\partial P_v}\right) \\ &\quad \left.+\lambda_v \left(\frac{Q}{g \sin\theta} - \lambda \rho_v \frac{\partial T}{\partial P_v}\right)\right], \\ \mathcal{H}^* &= -g \sin\theta \left[\lambda_l \lambda_v \rho_v h_{vl} + \lambda_l \left(\frac{Q}{g \sin\theta} + \frac{\rho_l \lambda}{\frac{\partial P_c}{\partial S}} \frac{\partial T}{\partial S}\right)\right. \\ &\quad \left.+\lambda_v \rho_v \lambda \frac{\partial T}{\partial S} \Big/ \frac{\partial P_c}{\partial S}\right], \\ P_v^* &= P_v / P_0, \\ z^* &= z / P_0, \\ \epsilon &= \frac{1}{P_0} \frac{\partial P_c}{\partial S}. \end{aligned}$$

B NOMENCLATURE

d	unit of permeability, 1 darcy $= 10^{-12}\mathrm{m}^2$
h	specific enthalpy
h_{vl}	latent heat of vaporization
g	gravitational acceleration
J	the Leverett J-function, $1.417(1-\mathrm{s}) - 2.12(1-s)^2 + 1.263(1-s)^3$
k	permeability

k_r	relative permeability
md	millidarcy, 10^{-3} darcy
m_l	molecular weight of liquid water (kg/kmol)
u	mass flux density (kg s^{-1} m^{-2})
P	pressure
P_c	capillary pressure
Q	energy flux (W/m^2)
R	gas constant (m^3 Pa K^{-1} mol–')
S	liquid saturation
T	temperature (°C)
z	vertical distance *(m)*

Greek symbols

β	ν_l/ν_v
γ	$\frac{dT}{dP}(\nu_v)/(h_{vl}\triangle\rho)$
λ	thermal conductivity
λ_l	liquid mobility, kk_{rl}/ν_l
λ_v	vapor mobility, kk_{rv}/ν_v
μ	dynamic viscosity
ν	kinematic viscosity
w	dimensionless heat flow ($Q\nu_v/(kgh_{vl}\triangle\rho$)
ϕ	porosity
ρ	specific density
σ	surface tension (Kg/s^2)

Subscripts

l	liquid water
v	steam or vapor phase